

Petascale computations for Large-scale Atomic and Molecular collisions

Brendan M McLaughlin and Connor P Ballance

Abstract Petaflop architectures are currently being utilized efficiently to perform large scale computations in Atomic, Molecular and Optical Collisions. We solve the Schrödinger or Dirac equation for the appropriate collision problem using the R-matrix or R-matrix with pseudo-states approach. We briefly outline the parallel methodology used and implemented for the current suite of Breit-Pauli and DARC codes. Various examples are shown of our theoretical results compared with those obtained from Synchrotron Radiation facilities and from Satellite observations. We also indicate future directions and implementation of the R-matrix codes on emerging GPU architectures.

1 Introduction

Our research efforts continue to focus on the development of computational methods to solve the Schrödinger and Dirac equations for atomic and molecular collision processes. Access to leadership-class computers allows us to benchmark our theoretical solutions against dedicated collision experiments at synchrotron facilities such as the Advanced Light Source (ALS), Astrid II, BESSY II, SOLEIL and Petra III and to provide atomic and molecular data for ongoing research in laboratory and astrophysical plasma science. In order to have direct comparisons with experiment, semi-relativistic or fully relativistic computations, involving a large number of target-coupled states are required to achieve spectroscopic accuracy. These com-

Brendan M McLaughlin

Centre for Theoretical Atomic, Molecular and Optical Physics (CTAMOP), School of Mathematics & Physics, The David Bates Building, Queen's University, 7 College Park, Belfast BT7 1NN, UK, e-mail: b.mclaughlin@qub.ac.uk

Connor P Ballance

Department of Physics, 206 Allison Laboratory, Auburn University, Auburn, AL 36849, USA e-mail: ballance@physics.auburn.edu

putations could not be even attempted without access to HPC resources such as those available at leadership computational centers in Europe and the USA. We use the R-matrix, R-matrix with pseudo-states (RMPS) method to solve the Schrödinger and Dirac equations for atomic and molecular collision processes.

Satellites such as *Chandra* and *XMM-Newton* are currently providing a wealth of x-ray spectra on many astronomical objects, but a serious lack of adequate atomic data, particularly in the *K*-shell energy range, impedes the interpretation of these spectra. Spectroscopy in the soft x-ray region (0.5–4.5 nm), including *K*-shell transitions of singly and multiply charged ionic forms of atomic elements such as Be, B, C, N, O, Ne, S and Si, as well as L-shell transitions of Fe and Ni, provides a valuable probe of the extreme environments in astrophysical sources such as active galactic nuclei (AGN's), x-ray binary systems, and cataclysmic variables [1, 2, 3]. For example, *K*-shell photoabsorption cross sections for the carbon isonuclear sequence have been used to model the Chandra X-ray absorption spectrum of the bright blazar Mkn 421 [4].

The motivation for our work is multi-fold; (a) Astrophysical Applications [5], (b) Fusion and plasma modelling, JET, ITER, (c) Fundamental interest and (d) Support of experimental measurements and Satellite observations. In the case of heavy atomic systems [6, 7], little atomic data exists and our work provides results for new frontiers on the application of the R-matrix; Breit-Pauli and DARC parallel suite of codes. The current state of parallelism for these codes is outlined and some indication of new directions being explored with emerging architectures is presented. These highly efficient codes are widely applicable to the support of present experiments being performed at synchrotron radiations facilities such as; ALS, ASTRID II, SOLEIL, PETRA III, BESSY II. Various examples of large scale calculations are presented to illustrate the predictive nature of the method.

The main question asked of any method is, how do we deal with the many bodied problem? In our case we use first principle methods (ab initio) to solve our dynamical equations of motion. Ab initio methods provides highly accurate, reliable atomic and molecular data (using state-of-the-art techniques) for solving the Schroedinger and Dirac equation. The R-matrix non-perturbative method is used to model accurately a wide variety of atomic, molecular and optical processes such as; electron impact ionization(EII), electron impact excitation (EIE), single and double photoionization and inner-shell X-ray processes. The R-matrix method provides highly accurate cross sections and rates used as input for astrophysical modelling codes such as; CLOUDY, CHIANTI, AtomDB, XSTAR that are necessary for interpreting experiment/satellite observations of astrophysical objects and fusion and plasma modeling for JET and ITER.

After the Iron Project one needs to proceed with the Trans-Iron Peak Elements; (Trans-Iron Peak Project: TIPP), since various UV spectra of hot post-AGB stars exhibit unidentified lines. Some of these lines may stem from highly ionized (VI-VIII) metals that are enriched by the *s*-process from atomic elements such as: Ge, Ba, Sr, Y, Pb. Determination of abundances would be most useful for these elements. However lines from such ions, are hitherto not identified as the main problem is precise wavelengths are required for unambiguous line

identifications. Some examples are, Ge, Pb, ..., in cooler white dwarfs and sub-dwarfs, however abundances are useless in these cases because they are strongly affected by diffusion. Palmeri and co-workers have initiated the DESIRE project (<http://w3.umons.ac.be/astro/desire.shtml>) to address the current deficiency of atomic data for such heavy atomic elements.

2 Parallel R-matrix Photoionization

The use of massively parallel architectures allows one to attempt calculations which previously could not have been addressed. This approach enables large scale relativistic calculations for trans-iron elements such as ; Kr-ions, Xe-ions [6]. It allows one to provide atomic data in the absence of experiment and takes advantage of the Linear algebra libraries available on most architectures. We fill in our sea of ignorance i.e. provide data on atomic elements where none have previously existed. The present approach has the capability to cater for Hamiltonian matrices in excess of 250 K x 250 K. Examples will be shown in the following sections for both valence and inner-shell photoionization for systems of prime interest to astrophysics and for more complex species necessary for plasma modelling in fusion tokamaks.

The development of the dipole codes, benefit from similar modifications and developments made to the existing excitation R-matrix codes. In this case all the eigenvectors from a pair of dipole allowed symmetries are required for bound-free dipole matrix formation. Every dipole matrix pair is carried out concurrently with groups of processors assigned to an individual dipole. The method is applicable to photoionization, dielectronic-recombination or radiation damped excitation and now reduces to the time taken for a single dipole formation. The method so far implemented on various parallel architectures has the capacity to cater for photoionization calculations involving 500 - 1000 levels. This dramatically improves (a) the residual ion structure, (b) ionization potential, (c) resonance structure and (d) can deal with in excess of 4,000 channels.

3 Scalability

As regards to the scalability of these R-matrix codes, we find from experience on a variety of petaflop machines that various modules within this suite of codes scale very well, upwards to 100,000 cores. In practical calculations for cross sections on various systems it is necessary to perform fine energy resolution of resonance features (10^{-8} (Ry) ~ 1.36 meV) which is observed in photoionization cross sections. This involves many (6 - 30 million) incident photon energies, vital when comparing with high precision measurements such as those performed on Xe⁺ at the Advanced Light Source synchrotron radiation facility in Berkeley, California, USA where energy resolutions of 4 - 9 meV FWHM are achieved.

The formation of many real symmetric matrices (Hamiltonians), typically 60 K -150 K, requires anywhere from 10-500 Gb of storage. The diagonalization of each matrix, from which *every* eigenvalue and *every* eigenvector is required is achieved through use of the ScaLapack package. In particular routines : **pdsyevx** and **pdsyevd**, where preference is given to the latter, as it ensures orthogonality between all eigenvectors. In typical collision calculations matrices vary in size from $2K \times 2K$ to $200K \times 200K$, depending on the complexity of the atomic target. The formation of the continuum-continuum part of the $N+1$ electron Hamiltonian is the most time consuming. Therefore if there are several thousand scattering channels then there are $[nchan \times (nchan + 1)/2]$ matrix blocks. Each block represents a partial wave and each subgroup reads a signal Hamiltonian and diagonalizes it in parallel, concurrently with each other. So there is endless scalability. R-matrix close-coupling calculations are therefore reduced to the time required for a single partial wave.

In Table 1 we show details of test runs for the outer region module PSTBF0DAMP for K-shell Photoionization of B II using 249-coupled states with 400 coupled channels and for 409,600 energy points and an increasing number of CPU cores. A factor of 4 speed up is achieved by using up to 8192 cores. The computations were carried out on the Cray-XE6 (Hopper) at NERSC. Note, for actual production runs, timings would be a factor of 10 larger, as one would require a mesh of 4,096,000 energy points to fully resolve the resonances features observed in the spectrum. We present the timings for core sizes varying from 1024 to 8192 again for B II K-shell photoionization in its ground state. The computations were done with the outer region module PSTGBF0DAMP for 249-states and 400-coupled channels.

Table 1 B II 249-states, 400 coupled channels, 409,600 energy points running on increasing number of cores. The results are from module PSTGB0FDAMP for photoionization cross-section calculations of the B II ion carried out on HOPPER the Cray XE6 at NERSC. Results are presented indicating the speed up factor with increasing number of CPU cores and the total number of core hours.

CRAY-XE6 CPU cores	PSTGB0FDAMP Absolute timing (s)	PSTGB0FDAMP Speed Up Factor	PSTGB0FDAMP Total Core hours
1024	584.19	1.0000	166.1155
2048	430.80	1.3584	245.0077
4096	223.08	2.6183	253.8154
8192	149.70	3.9018	340.6506

The main work horse in our linear algebra code is the ScaLAPACK libraries. The goals of the ScaLAPACK project are the same as those of LAPACK; Efficiency (to run as fast as possible), Scalability (as the problem size grows so do the numbers of processors grow), Reliability (including error bounds), Flexibility (so users can construct new routines from well-designed parts) and Ease of Use (by making the interface to LAPACK and ScaLAPACK look as similar as possible). Many of these goals, particularly portability are aided by developing and promoting standards, especially for low level communication and computation routines.

Parallel I/O issues have been addressed for the photoionization module, PSTGBF0DAMP, as several large passing files (ranging from 10 Gb to -150 Gb) need to be read during runtime. These files are SEQUENTIAL FORTRAN BINARY files. For large-scale computations using the module PSTGBF0DAMP, file names have a typical size, e.g. Hamiltonian file : H.DAT (10-150 Gb), dipole files : D00,D01,D02,D03,, DNN (2 - 50 Gb). Traditionally, all processors read these files together. For a small numbers of processors, say less than 500 processors and file sizes (< 5 Gb) both on the Hopper Cray XE6 (NERSC) and the Kraken Cray XT5 (National Institute for Computational Science, NICS) architectures, the jobs perform well, with the I/O time being $< 10\%$ of the total wall clock time. However, as the number of processors increases, i.e 5000-6000 processors, the I/O percentage of wall clock time is typically 33% pre-striping. This I/O issue has been addressed using efficient striping of the data files. The Lustre file system is made up of an underlying set of I/O servers and disks called Object Storage Servers (OSSs) and Object Storage Targets (OSTs) respectively. A file is said to be striped when read and write operations access multiple OST's concurrently. File striping is used to increase the I/O performance of our codes writing or reading from multiple OST's simultaneously increases dramatically the available I/O bandwidth. We have investigated the following I/O issues along with the use of striping files.

1. The H.DAT file, unlike the D00,D01, ... files is read sequentially from start to finish by all processors, however by allowing ONLY processor 0 to read, then distribute (i.e. MPLBCAST) the information to the remaining processors is a better solution. This technique however cannot be implemented for the dipole (DXX) files, as each processor is reading different parts of the file, and different amounts of information at each read. Table 2 shows the minimal increase in performance for module PSTGBF0DAMP for the large-scale photoionization cross-section calculations on Ca II using this approach.
2. Each DXX file holds enough information to describe the photoionization process from the ground state and ALL excited states of an atom/ion. If the user/scientist requires only a small subset of all possible photoionization cross sections, (i.e. ground-state and first metastable) then the DXX files could be REDUCED in size.
3. Modification of the directory structure on the LUSTRE filesystem, so that the large files may be efficiently STRIPED increases the I/O performance of our codes. We have carried out various striping investigations in collaboration with a computational scientist consultant Vince Betro, at NICS, to optimize the 'best striping' based on file size. Furthermore detailed testing has been done on the Cray XE6 at NERSC (Hopper), the Cray XT5 at NICS (Kraken). and on the Cray XE6 at HLRS (Hermit), in Stuttgart, Germany. Our findings are as follows. For file sizes of < 1 Gb, we use the default striping of files (Hopper has a values of 2, Kraken a value of 1, Hermit a value of 4). For file sizes of between 1 Gb - 10 Gb we use small stripling values, typically 20 gives optimal throughput depending on the system load, which is only apparent at the NICS facility. In the case of file sizes between 10 Gb - 100 Gb a medium stripling value of 60 appears to be optimal. For files in excess of 100 Gb a striping value of 120 was used.

Table 2 Ca II, 513-states, 1815 coupled channels, 6,000 energy points running on 6,000 cores. The results are from module PSTGBF0DAMP for photoionization of Ca II carried out on HOPPER the Cray XE6 at NERSC.

CRAY-XE6 Ca II	PSTGBF0DAMP ^a Absolute timings (s)	PSTGBF0DAMP ^b Absolute timings (s)
6000 cores	108.2344 ^c	116.2098
maximum coupled channels	1815	1815
D file size	6 Gb	6Gb
H matrix size	23073	23073

^a with READ/MPI.BCAST

^b without READ/MPI.BCAST

^c Time in seconds

Optimization of the R-matrix codes on a variety of HPC architectures implements several good coding practices. We use code inlining (which reduces overhead from calling subroutines), loop unrolling, modularization, unit strides, vectorization and dynamic array passing. Highly optimized libraries such as; ScaLapack, BLAS and BLACS are used extensively in the codes. On Cray architectures, the R-matrix codes are profiled with performance utilities such as CrayPat and IPM which gives the user an indication of their scalability. Standard MPI/FORTRAN 90/95 programming is used on the world’s leading-edge petaflop high performance supercomputers. Serial (legacy) code to parallel R-matrix implementation is carried out using a small subset of basic MPI commands.

4 X-ray and Inner-Shell Processes

To measure the chemical evolution of the universe and then understand its ramifications for the formation and evolution of galaxies and other structures is a major goal of astrophysics today. *HUT* and *IUE* observations have been used to study the processing and dredging that goes on during the lifetime of a star. Gas that is photoionized by a hard radiation field (AGN/quasars, IGM, cataclysmic variables, X-ray binaries, etc...) can be stripped of its inner-shell electrons, and several phenomenon then occur which can radically alter the ionization balance of the gas. Space-based UV observations of emission and absorption lines from ions of C, N, O, S and Si in photoionized sources play an important role in addressing many of the astrophysical issues listed above.

Absolute *K*-shell photoionization cross sections for atomic nitrogen have been obtained from high resolution experiment at the ALS and the R-matrix with pseudo-states approach (RMPS). Due to the difficulty of creating a target of neutral atomic nitrogen, no high-resolution *K*-edge spectroscopy measurements have been reported for this important atom. Interplay between theory and experiment enabled identification and characterization of the strong $1s \rightarrow np$ resonance features throughout

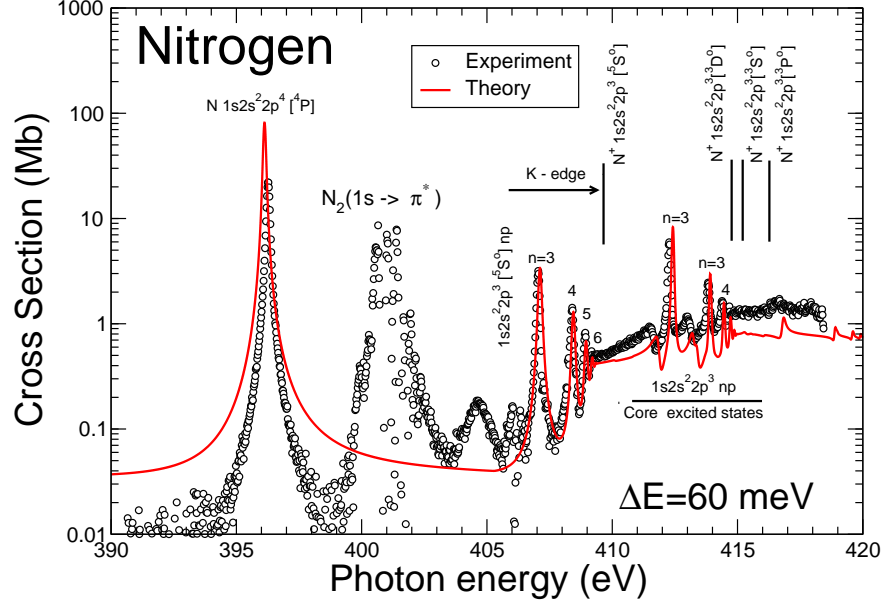


Fig. 1 Atomic-nitrogen total photoionization cross section. Theoretical results from the R-matrix with pseudo-states method (RMPS) were convoluted with a 60 meV FWHM Gaussian to simulate the ALS experiment. Experimental results include molecular components between 400 and 406 eV [8].

the threshold region. An experimental value of 409.64 ± 0.02 eV was determined for the K -shell binding energy. Fig 1 illustrates the comparison between theory and experiment in the K -shell region from our recent work on this system [8].

An accurate description of the photoionization/photoabsorption of atomic oxygen is important for a number of atmospheric and astrophysical applications. Photo-absorption of atomic oxygen in the energy region below the $1s^{-1}$ threshold in x-ray spectroscopy from *Chandra* and *XMM-Newton* is observed in a variety of x-ray binary spectra. Photo-absorption cross sections determined from an R-matrix method with pseudo-states (RMPS) and high precision measurements from the Advanced Light Source (ALS) are presented in Fig. 2. High-resolution spectroscopy with $E/\Delta E \approx 4,250 \pm 400$ were obtained for photon energies from 520 eV to 555 eV at an energy resolution of 124 ± 12 meV FWHM. K -shell photoabsorption cross-section measurements were made with on atomic oxygen at the ALS. Natural line widths Γ are extracted for the $1s^{-1}2s^22p^4(^4P)np\ ^3P^o$ and $1s^{-1}2s^22p^4(^2P)np\ ^3P^o$ Rydberg resonances series and compared with theoretical predictions. Accurate cross sections and line widths are obtained for applications in x-ray astronomy. Excellent agreement between theory and the ALS measurements is shown which will have profound implications for the modelling of x-ray spectra and spectral diagnostics. Further details can be found in our recent study on this complex [9].

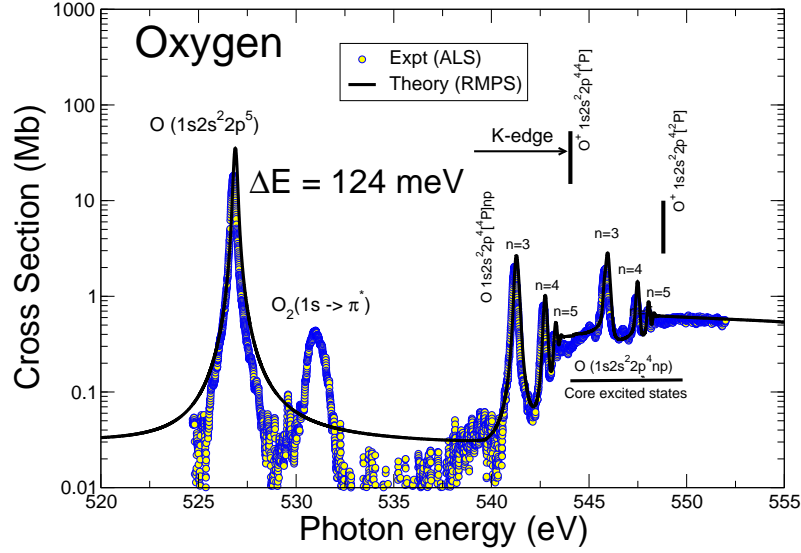


Fig. 2 (Colour online) Atomic oxygen photo-absorption cross sections taken at 124 meV FWHM compared with theoretical estimates. The R-matrix calculations shown are from the R-matrix with pseudo-states method (RMPS: solid black line, present results) convoluted with a Gaussian profile of 124 meV FWHM [9].

5 Heavy atomic systems

5.1 Kr and Xe ions

Photoionization cross sections of heavy atomic elements, in low stages of ionization, are currently of interest both experimentally and theoretically and for applications in astrophysics. The data from such processes have many applications in planetary nebulae, where they are of use in identifying weak emission lines of n -capture elements in NGC 3242. For example, the relative abundances of Xe and Kr can be used to determine key physical characteristics of s -process nucleosynthesis, such as the neutron exposure experienced by Fe-peak seed nuclei.

Xenon and Krypton ions are also of importance in man-made plasmas such as XUV light sources for semiconductor lithography, ion thrusters for space craft propulsion and nuclear fusion plasmas. Xenon and Krypton ions have also been detected in cosmic objects, e.g., in several planetary nebulae and in the ejected envelopes of low- and intermediate-mass stars [6].

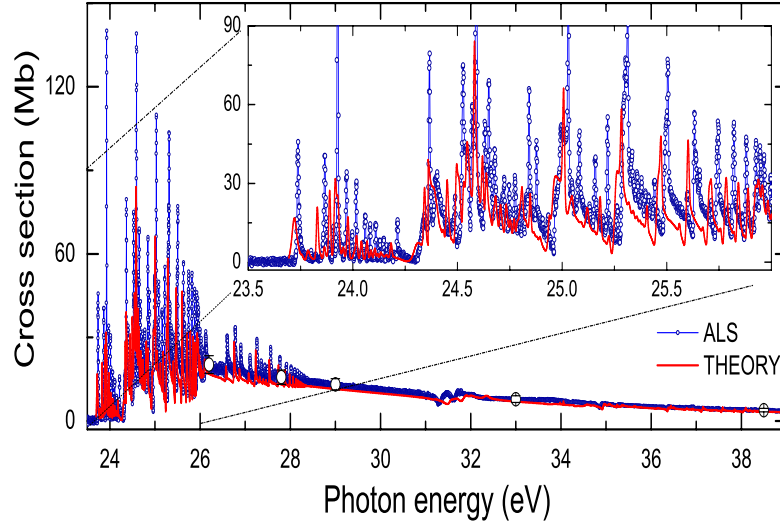


Fig. 3 An overview of measurements for the absolute single photoionization measurements of Kr^+ ions as a function of the photon energy measured with theoretical estimates for cross sections. The ALS measurements are at a nominal energy resolution of 7.5 meV and normalized to the ASTRID/SOLEIL measurements at 26.5025 eV. Theoretical results were obtained from a Dirac-Coulomb R-matrix method, convoluted with the appropriate Gaussian of FWHM and a statistical admixture of 2/3 ground and 1/3 metastable states [10].

We apply the suite of DARC codes to calculate detailed photoionization (PI) cross sections on the halogen-like ions, Kr^+ and Xe^+ . Photoionization (PI) cross section calculations on the Kr^+ complex were carried out retaining 326-levels in our close-coupling calculations with the Dirac-Atomic-R-matrix-Codes (DARC). In R-matrix theory, all photoionization cross section calculations require the generation of atomic orbitals based primarily on the atomic structure of the residual ion. The present theoretical work for the photoionization of the Kr^+ ion employs relativistic atomic orbitals up to $n=4$ generated for the residual Kr^{2+} ion, which were calculated using the extended-optimal-level (EOL) procedure within the GRASP structure code[6].

Fig. 3 shows the comparison of our large-scale (326-levels) photoionization cross section calculations for Kr^+ ions with the DARC suite of codes compared with the high resolution measurements carried out at the Advanced Light Source (ALS), in Berkeley, California, USA. It is clearly see from Fig. 3 that our results obtained using the DARC codes reproduce all the fine detail resonance features in the observed

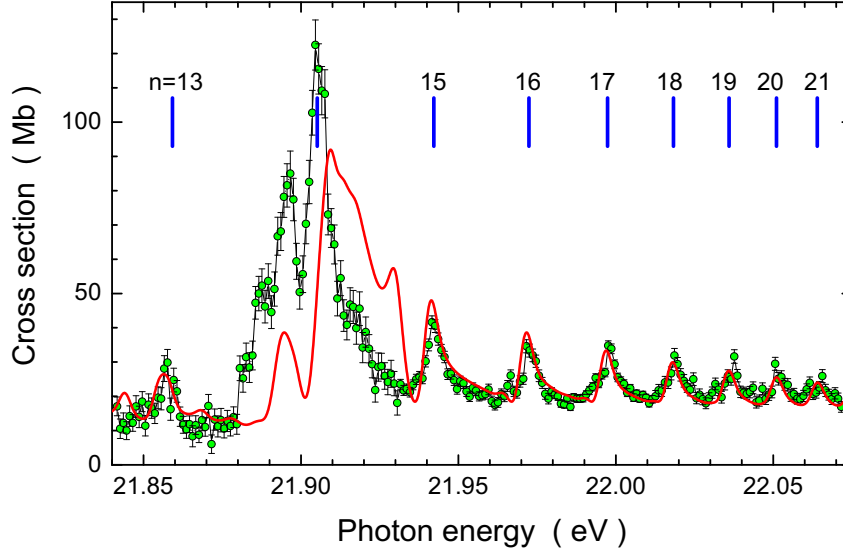


Fig. 4 Xe^+ ALS experimental PI cross section data (green circles) for photon energies ranging from 21.84 eV - 22.08 eV at a photon energy resolution of 4 meV. Results are compared with theoretical results from a 326-level Dirac-Coulomb R-matrix calculation (red line) convoluted with a FWHM Gaussian of 4 meV and statistically averaged over the ground and metastable states to simulate the experimental measurements. The bars mark the energies of the $[5s^2 5p^4 (^3P_1) nd]$ resonances obtained with a quantum defect of 0.16. [7]

spectra obtained in the ALS measurements over the photon energy range investigated [10].

Similarly photoionization cross section calculations on the Xe^+ system retained 326 levels of the residual Xe^{2+} ion in our close-coupling calculations performed with the Dirac-Atomic-R-matrix-Codes (DARC). For the Xe^+ case we have employed relativistic $n=5$ atomic orbitals generated for the residual Xe^{2+} ion, which were obtained using the energy-average-level (EAL) procedure within the GRASP structure code on the fourteen lowest levels associated with the $5s^2 5p^4$, $5s 5p^5$ and $5s^2 5p^3 5d^2$ configurations. For Xe^+ ions a more stringent test with recent extremely high resolution experimental measurements made at the ALS at 4 meV as illustrated in Fig. 4 indicate (in the near threshold region, apart from the $n=14$ member of the Rydberg series) very good agreement giving us confidence in our theoretical results [6].

5.2 Tungsten (W) Ions

The choice of materials for the plasma facing components in fusion experiments is guided by competing desirables: on the one hand the material should have a high thermal conductivity, high threshold for melting and sputtering, and low erosion rate under plasma contact, and on the other hand as a plasma impurity it should not cause excessive radiative energy loss. The default choice of material for present experiments is carbon (or graphite), however tritium is easily trapped in carbon-based walls and for that reason carbon is at present held to be unacceptable for use in a D-T fusion experiment such as ITER, under construction in Cadarache, France, or in a fusion reactor. In its place, tungsten (symbol W, atomic number 74) is the favoured material for the wall regions of highest particle and heat load in a fusion reactor vessel, with beryllium a possibility for regions of lower heat and particle load. ITER is scheduled to start operation with a W-Be-C wall for a brief initial campaign before switching to W-Be or W alone for the main D-D and D-T experimental program. In support of ITER and looking ahead to a fusion reactor the ASDEX-Upgrade tokamak now operates with an all-W wall, and at JET a full ITER-like mixed W-Be-C wall is being installed. Smaller-scale experiments involving tungsten tiles are carried out on other tokamaks. The attractiveness of tungsten is due to its high thermal conductivity, its high melting point, and its resistance to sputtering and erosion, and is in spite of a severe negative factor that as a high-Z plasma impurity tungsten does not become fully stripped of electrons and radiate copiously, so that the tolerable fraction of tungsten impurity in the plasma is at most 2×10^{-5} .

The walls of ITER are coated with tungsten which can therefore enter the fusion plasma. W ions impurities in a fusion plasma causes critical radiation loss and minuscule concentrations prevent ignition. High resolution experiments are currently available from the ALS on low ionization stages of W ions. We use the Dirac-Atomic-R-matrix-Codes (DARC) to perform large scale calculations for the single photoionization process and compare our results with experiment. These systems are an excellent test bed for the photoionization (PI) process where excellent agreement is achieved between theory and experiment providing a road-map for electron - impact excitation (EIE).

For photoionization of the W^{3+} ion of tungsten we investigated several different scattering models before settling on a 379 level model obtained from 9 configuration state functions of the residual ion. Fig. 5 shows our theoretical results from this 379-level model obtained from the DARC codes compared with measurements made at the Advanced Light source. From the the comparison made in Fig. 5 suitable agreement with the ALS experimental measurements is obtained when the theoretical results are statistically averaged over the fine-structure levels. Additional ions of tungsten are presently being explored and will be reported on in due course.

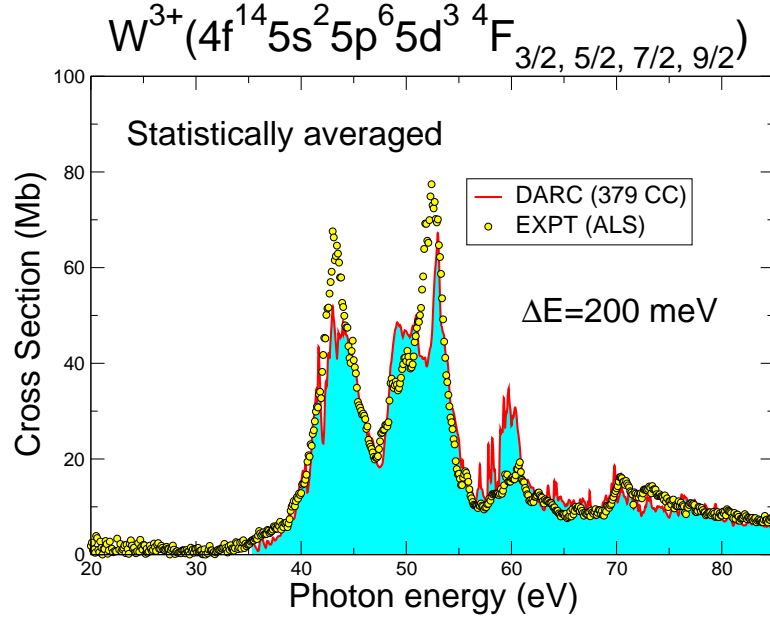


Fig. 5 Photonization of W^{3+} ions over the photon energy range 20 eV - 90 eV. Theoretical work (solid red line: DARC) from the 379 level approximation calculations, convoluted with a Gaussian profile of 200 meV FWHM and statistically averaged over the fine structure $J = 3/2, 5/2, 7/2$ and $9/2$ levels (see text for details). The solid circles (yellow) are from the experimental measurements made at the ALS using a band width of 200 meV.

6 Future directions and emergence of GPUS

Experience with the test bed machine DIRAC at NERSC, a 50 core GPU architecture and the Cray XK7 (TITAN) at ORNL has indicated various things. MPI/Fortran codes access the GPU (Graphical Processing Unit) through the PGI CUDA fortran compiler and an architecture supporting NVIDIA graphics cards. Those using C/C++ have greater flexibility. One of the issues is identifying an intensive numerical algorithm within your code that would benefit from distribution across one or more GPUS. GPUS may be slower than their equivalent CPUS but there are many more cores. One success has been the formation of the R-matrix itself, which may be expressed as a matrix multiplication that has to be carried out repeatedly which occurs in the outer region module PSTGF. The NVIDIA kepler GPUS on DIRAC outperformed the optimized LAPACK routine DGEMM by a factor of eight, though there is still room to improve the code with CUDA BLAS. Hence formation of the R-matrix

$$R_{ij} = \sum_k \frac{W_{ik} \times W_{kj}}{(E - E_k)} \quad (1)$$

is essentially a matrix multiplication

$$\mathbf{R} = \mathbf{X} \times \mathbf{Y} \quad (2)$$

where the elements of \mathbf{R} are R_{ik} , \mathbf{X} are $w_{ik}/(E - E_k)$ and \mathbf{Y} are w_{kj} .

Table 3 Range of timings (in seconds) using DGEMM for matrix multiplication and the ratio of CPU:GPU on the Cray XK7 (TITAN) leadership computational architecture located at Oak Ridge National Laboratory. The results are from module PSTGF and for electron scattering for Fe III.

Matrix multiplication $n \times m$	CPU:GPU 1:1	CPU:GPU 2:1	CPU:GPU 4:1
267×16512	0.24 ^a	0.35	0.30
308×19201	0.72	0.52	0.52
399×24666	0.51	1.10	1.12
526×32530	0.04	0.06	0.68
132×8155	0.22	0.32	0.06
260×16102	0.90	1.21	0.33
837×51573	1.03	1.40	1.71
796×49169	3.43	1.40	1.84
1368×84321	3.43	4.60	—
1241×76646	2.73	3.70	—

^a Time in seconds

One of the underlying questions is, how will performance degrade as CPU/GPU ratio increases? On TITAN, the Oak Ridge National Laboratory leadership computational facility, which has a heterogeneous environment (CPU/GPU), a range of timings using DGEMM and the ratio of CPU:GPU were investigated for the outer region module, PSTGF. We investigated the case of electron scattering from the Fe III ion. Ten different matrix sizes were investigated with 16 MPI tasks, therefore the MPI process carries out 160 multiplies of each matrix. Table 3 shows the results for these timings for the increasing CPU: GPU ratio and increasing matrix size.

Acknowledgements C P Ballance was supported by US Department of Energy (DoE) grants through Auburn University. B M McLaughlin acknowledges support by the US National Science Foundation through a grant to ITAMP at the Harvard-Smithsonian Center for Astrophysics and a visiting research fellowship from Queen’s University Belfast. The computational work was carried out at the National Energy Research Scientific Computing Center in Oakland, CA, USA, the Kraken XT5 facility at the National Institute for Computational Science (NICS) in Knoxville, TN, USA and at the High Performance Computing Center Stuttgart (HLRS) of the University of Stuttgart, Stuttgart, Germany. The Kraken XT5 facility is a resource of the Extreme Science and Engineering Discovery Environment (XSEDE), which is supported by National Science Foundation grant number OCI-1053575. This research also used resources of the Oak Ridge Leadership Computing Facility at the Oak Ridge National Laboratory, which is supported by the Office of Science of the U.S. Department of Energy under Contract No. DE-AC05-00OR22725.

References

1. McLaughlin, B. M.: Inner-shell Photoionization, Fluorescence and Auger Yields. In: Ferland, G. and Savin, D. W. (eds) *Spectroscopic Challenges of Photoionized Plasma*, Astronomical Society of the Pacific, ASP Conf. Series **247** pp. 87. San Francisco (2001)
2. Kallman, T. R.: Challenges of Plasma Modelling: Current Status and Future Plans. *Space Sci. Rev.* **157**, 177 (2010)
3. McLaughlin, B. M. and Ballance, C. P.: Photoionization, Fluorescence and Inner-shell Processes. In: McGraw-Hill (eds) *McGraw-Hill Yearbook of Science and Technology*, pp. 281. McGraw Hill, New York (2013)
4. Hasoglu, M. F. Abdel, Naby S. A., Gorczyca, T. W., Drake J. J. and McLaughlin, B. M. : K-shell Photoabsorption Studies of the Carbon Isonuclear Sequence. *Astrophys. J.* **724**, 1296 (2010)
5. Covington, A. M., Aguilar, A., Covington, I. R., Hinojosa, G., Shirley, C. A., Phaneuf, R. A., Álvarez, I., Cisneros, C., Dominguez-Lopez, I., Sant'Anna, M. M., Schlachter, A. S., Ballance, C. P. and McLaughlin, B. M.: Valence-shell photoionization of chlorinelike Ar^+ ions. *Phys. Rev. A* **84**, 013413 (2011)
6. McLaughlin, B. M. and Ballance, C. P.: Photoionization cross section calculations for the halogen-like ions Kr^+ and Xe^+ . *J. Phys. B: At. Mol. Opt. Phys.* **45**, 085701 (2012)
7. McLaughlin, B. M. and Ballance, C. P.: Photoionization Cross-Sections for the trans-iron element Se^+ from 18 eV to 31 eV. *J. Phys. B: At. Mol. Opt. Phys.* **45**, 095202 (2012)
8. Sant'Anna, M. M., Schlachter, A. S., Öhrwall, G., Stolte, W. C., Lindle, D. W. and McLaughlin, B. M. : K-shell X-ray Spectroscopy of Atomic Nitrogen, *Phys. Rev. Lett.* **107**, 033001 (2011)
9. McLaughlin, B. M., Ballance, C. P., Bown, K. P., Gardenghi, D. J. and Stolte, W. C.: High Precision K-shell Photoabsorption Cross Sections for Atomic Oxygen: Experiment and Theory. *Astrophys. J.* **771**, L8 (2013)
10. Hinojosa, G., Covington, A. M., Alna'Washi, G. A., Lu, M., Phaneuf R. A., Sant'Anna, M. M., Cisneros, C., Álvarez, I., Aguilar, A., Kilcoyne, A. L. D., Schlachter, A. S., Ballance, C. P. and McLaughlin, B. M. : Valence-shell photoionization of Kr^+ ions: Experiment and Theory. *Phys. Rev. A* **86**, 063402 (2012)